Generalized Sail Trajectory Approximation with Applications to MagSails

Marco Bassetto*, Alessandro A. Quarta, Giovanni Mengali

Dipartimento di Ingegneria Civile e Industriale, University of Pisa, Italy

Abstract

This paper investigates approximate solutions to the two-dimensional equations of motion of a generalized sail-based spacecraft. A generalized sail is a propellantless propulsion system that produces a continuous thrust the magnitude of which varies with the heliocentric distance as $1/r^\eta$, where η is a positive real number that characterizes the propulsion system performance. Under the simplifying assumptions of low propulsive acceleration, constant thrust angle, and circular parking orbit, the spacecraft trajectory is approximated through closed-form relations. The general solution is then specialized to the case of a Magnetic Sail with a so-called "thick" operation mode, the latter being consistent with a kilometer-size loop radius. The effectiveness of the proposed mathematical model is verified by comparison with a numerical integration of the equations of motion, which confirms the accuracy of the analytical results even on very long timescales. Finally, the set of approximate equations is applied to the analysis of transfer trajectories towards a heliocentric target orbit with a given semimajor axis.

Keywords: generalized sail, MagSail, trajectory approximation

Nomenclature

a	=	semimajor axis, [au]
a_c	=	characteristic acceleration, [mm/s^2]
$\boldsymbol{a}$	=	propulsive acceleration vector, [mm/s^2]
$\{C_D,\, C_L\}$	=	dimensionless functions of ϕ
h	=	spacecraft specific angular momentum magnitude, [km^2/s]
$\{h_0,\, h_1\}$	=	best fit coefficients of C_D
$\hat{\boldsymbol{\imath}}_r$	=	radial unit vector
$\hat{\boldsymbol{\imath}}_\theta$	=	transverse unit vector
$\{k_0,\, k_1\}$	=	best fit coefficients of C_L
$\boldsymbol{m}$	=	magnetic dipole moment, [A m^2]
O	=	Sun's center of mass
r	=	Sun-spacecraft distance, [au]
$\boldsymbol{r}$	=	spacecraft position vector, [au]
$r_\oplus$	=	reference distance, [au]
S	=	spacecraft center of mass
t	=	time, [days]
$\mathcal{T}$	=	polar reference frame
$\boldsymbol{v}$	=	spacecraft velocity vector, [km/s]
v_r	=	radial component of spacecraft velocity, [km/s]

*Corresponding author

Email addresses: marco.bassetto@ing.unipi.it (Marco Bassetto), a.quarta@ing.unipi.it (Alessandro A. Quarta), g.mengali@ing.unipi.it (Giovanni Mengali)

Published in Aerospace Science and Technology, Vol. 118, November 2021, pp. 106991 (1–9). doi: https://doi.org/10.1016/j.ast.2021.106991

v_θ	=	transverse component of spacecraft velocity, [km/s]
α	=	thrust angle, [deg]
β	=	dimensionless coefficient, see Eq. (13)
γ	=	dimensionless function
ϵ_i	=	dimensionless relative error
η	=	dimensionless thruster parameter
θ	=	polar angle, [deg]
λ	=	dimensionless thruster coefficient, see Eq. (13)
$\mu_\odot$	=	Sun's gravitational parameter, [km^3/s^2]
ϕ	=	angle of attack, [rad]
χ	=	dimensionless auxiliary function, see Eq. (15)

Subscripts

0	=	initial
f	=	final
max	=	maximum
min	=	minimum

Superscripts

$\cdot$	=	time derivative
$\sim$	=	approximate

1. Introduction

The use of propellantless propulsion systems in the interplanetary space, such as photonic solar sails [1, 2, 3, 4, 5], Electric Solar Wind Sails (E-sails) [6, 7, 8, 9, 10], or magnetic sails (MagSails) [11, 12, 13], is a fascinating option in view of the opportunity they offer to obtain long-lasting missions. A common peculiarity of these propulsion systems is in the dependence of the thrust magnitude on the distance from the Sun. The thrust is obtained by exploiting the solar wind flux or the solar radiation pressure, so that the thrust vector can only point outward from the Sun's direction. All these propulsion systems may therefore be referred to as "generalized sails", a concept that was introduced by Aliasi et al. [14, 15, 16] about ten years ago to simulate the behaviour of photonic solar sails and E-Sails with a Sun-facing attitude. The original concept of generalized sail has also been recently used in Ref. [17] to investigate a new class of spiral trajectories covered by a radially-accelerated spacecraft with a constant mass.

The aim of this paper is to extend the mathematical model introduced by Aliasi et al. [14, 15, 16], and to look for approximate solutions to the two-dimensional equations of motion of a generalized sail-based spacecraft. The problem of developing approximate solutions to the spacecraft equations of motion is a very current topic, as is shown, for example, by Ogundele's recent work [18], which deals with the nonlinear Riccati spacecraft formation flying dynamics. Under the simplifying assumptions of low propulsive acceleration magnitude, constant thrust angle, and circular parking orbit, the spacecraft trajectory may be approximated through closed-form relationships. The general solution is then applied to the special case of a MagSail with a so-called "thick" operation mode, which is consistent with a MagSail with a kilometer-size loop radius. More precisely, a MagSail is constituted by a large ring made of superconducting material through which an electric current flows so as to generate a magnetic field. The interaction between the solar ions and the artificial magnetosphere surrounding the MagSail causes a momentum exchange and induces the onset of a thrust. The latter is nearly aligned with the Sun-spacecraft line, although a small transverse thrust component may also be obtained by suitably orienting the magnetic dipole moment. Figure 1 shows an artistic impression of the MagSail concept.

In the last two decades, several simulations and laboratory tests [19, 20, 21, 22] have provided important information about the MagSail theoretical performance. Starting from those data, Quarta et al. [23] have suggested a handy mathematical description of the MagSail thrust vector. This model has been recently

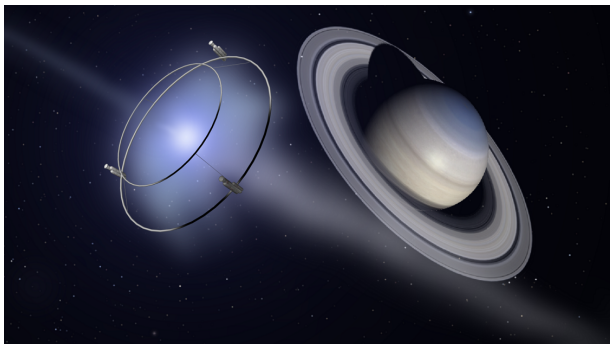

Figure 1: Artistic illustration of the MagSail concept. Courtesy of Steve Bowers, 2021.

used in Ref. [13] to analyze MagSail-based displaced non-Keplerian orbits around the Sun and, now, will be exploited to analyze heliocentric transfers by means of a low-performance MagSail. The effectiveness of the proposed solution is checked by comparison with the numerical integration of the equations of motion. In particular, the validity of the approximate model is investigated by quantifying the relative errors on a very long timescale.

The paper is organized as follows. Section 2 deals with the mathematical model used to describe the two-dimensional orbital dynamics of a spacecraft equipped with a generalized sail. Section 3 derives an analytical approximation of the propelled trajectory by introducing a set of suitable simplifying assumptions. Section 4 specializes the previously found results to the case of a MagSail with a "thick" magnetopause mode. The analytical model is then validated in Section 5, where a comparison between the approximate and numerical results confirms the accuracy of the proposed solutions. Section 6 investigates a set of transfer trajectories towards a target orbit with an assigned semimajor axis. Finally, Section 7 contains some concluding remarks, while the subsequent Appendix (Section 8) makes a comparison between the presented solutions and those available in the literature.

2. Mathematical preliminaries

Consider a heliocentric mission scenario in which, at the starting time $t_0 \triangleq 0$, a spacecraft S covers a circular Keplerian orbit of radius r_0. The magnitude of the spacecraft initial velocity is $v_0 \triangleq \sqrt{\mu_\odot / r_0}$, where $\mu_\odot$ is the Sun's gravitational parameter. Introduce a heliocentric polar reference frame $\mathcal{T}(O; \hat{\boldsymbol{\imath}}_r, \hat{\boldsymbol{\imath}}_\theta)$, where the origin O coincides with the Sun's center of mass, $\hat{\boldsymbol{\imath}}_r$ is the Sun-spacecraft (radial) unit vector, and $\hat{\boldsymbol{\imath}}_\theta$ is the transverse unit vector; see Fig. 2. The spacecraft position ($\boldsymbol{r}$) and velocity ($\boldsymbol{v}$) vectors in $\mathcal{T}$ are given by

$$\boldsymbol{r} = r\,\hat{\boldsymbol{\imath}}_r \quad , \quad \boldsymbol{v} = v_r\,\hat{\boldsymbol{\imath}}_r + v_\theta\,\hat{\boldsymbol{\imath}}_\theta \tag{1}$$

where r is the Sun-spacecraft distance, while v_r and v_θ are the radial and transverse component of the spacecraft velocity vector, respectively, which are defined as

$$v_r \triangleq \dot{r} \quad , \quad v_\theta \triangleq r\,\dot{\theta} \tag{2}$$

where θ is the spacecraft polar angle, measured anticlockwise from the Sun-spacecraft line at the initial time t_0; see Fig. 2.

The spacecraft dynamics is described by the polar equations of motion

$$\dot{r} = v_r \quad , \quad \dot{\theta} = \frac{h}{r^2} \quad , \quad \dot{v}_r = -\frac{\mu_\odot}{r^2} + \frac{h^2}{r^3} + \boldsymbol{a}\cdot\hat{\boldsymbol{\imath}}_r \quad , \quad \dot{h} = r\,\boldsymbol{a}\cdot\hat{\boldsymbol{\imath}}_\theta \tag{3}$$

where $h \triangleq r\,v_\theta$ is the magnitude of the specific angular momentum vector, while $\boldsymbol{a}$ is the propulsive acceleration vector. Note that the dynamical model described by Eqs. (3) does not consider the third-body perturbation effects. Such effects will be ignored throughout the paper because we are interested in analysing

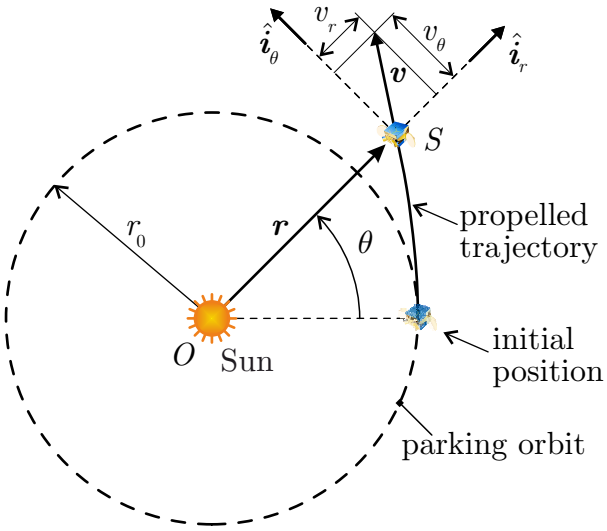

Figure 2: Reference frame and spacecraft state variables.

the heliocentric transfer phase of a generalized sail-based spacecraft, where the gravitational perturbations are small and, as such, of no practical interest in a preliminary phase of the trajectory analysis. In fact, the deep space phase represents a large part of an interplanetary transfer and, therefore, it is reasonable to neglect the gravitational perturbations due to the attraction of the departure and arrival planets. Bearing in mind that the parking orbit is circular, the system of differential equations (3) is completed by the following initial conditions

$$r(t_0) = r_0 \quad , \quad \theta(t_0) = 0 \quad , \quad v_r(t_0) = 0 \quad , \quad h(t_0) = r_0\, v_0 \equiv \sqrt{\mu_\odot\, r_0} \tag{4}$$

Assume now that the spacecraft is equipped with a primary propulsion system that may be considered as an extension of the "generalized sail" concept introduced by Aliasi et al. [14, 15, 16]. More precisely, according to the model discussed in Ref. [14], a generalized sail is essentially a propellantless propulsion system, capable of providing a continuous thrust in the interplanetary space by exploiting either the solar wind or the solar radiation pressure. A generalized sail typically gives an outward radial propulsive acceleration, the magnitude of which depends on the heliocentric distance as $1/r^\eta$, where $\eta \geq 0$ is a constant design parameter that characterizes the propulsion system. In particular, in the applications discussed by Aliasi et al. [14, 15, 16], the value of η is chosen so as to describe the behaviour of suitable propulsion systems, such as a photonic solar sail or an E-Sail with a Sun-facing attitude, that is, with a thrust vector aligned along the Sun-spacecraft line.

In this paper, the original concept of a generalized sail is extended by assuming a nonzero value of the transverse component of $\boldsymbol{a}$, that is, by considering the more general case in which $\boldsymbol{a} \cdot \hat{\boldsymbol{i}}_\theta \neq 0$. With the aim of describing the orbital dynamics of a spacecraft equipped with a propellantless thruster, the propulsive acceleration vector is here modeled as

$$\boldsymbol{a} = a_c\, \gamma \left(\frac{r_\oplus}{r}\right)^\eta \left(\cos\alpha\, \hat{\boldsymbol{i}}_r + \sin\alpha\, \hat{\boldsymbol{i}}_\theta\right) \tag{5}$$

where $a_c > 0$ is a reference propulsive acceleration (a sort of sail performance parameter) and $r_\oplus \triangleq 1\,\text{au}$ is a reference distance. In Eq. (5), the terms γ and α are related to the sail orientation relative to the local radial unit vector $\hat{\boldsymbol{i}}_r$. In particular, the dimensionless function $\gamma \in [\gamma_{\min}, 1]$ (with $\gamma_{\min} \geq 0$) models a possible dependence of the propulsive acceleration magnitude on the sail attitude, whereas $\alpha \in [-\alpha_{\max}, \alpha_{\max}]$ (with $\alpha_{\max} > 0$) is the thrust angle, that is, the angle between $\boldsymbol{a}$ and $\hat{\boldsymbol{i}}_r$. Using the standard nomenclature for photonic solar sails [1], a_c is referred to as "characteristic acceleration", since it coincides with the maximum magnitude of $\boldsymbol{a}$ (obtained when $\gamma = 1$) at the reference distance $r = r_\oplus$.

The values of $\{\eta,\, \alpha_{\max}\}$ and the expression of γ depend on the specific propulsion system that is modeled through the generalized sail concept. For example, the propulsive acceleration vector of a flat and perfectly reflective solar sail [24] is obtained with $\eta = 2$, $\alpha_{\max} = 90\,\text{deg}$, and $\gamma = \cos^2\alpha$, while the propulsive acceleration vector of Robert Forward's solar-photon thrustor [25, 26, 27] is characterized by $\eta = 2$, $\alpha_{\max} = 90\,\text{deg}$, and $\gamma = \cos\alpha$. Note that, in general, γ is not necessarily an explicit function of α. This is the case, for example, of the latest mathematical models that describe the propulsive acceleration vector generated by a spinning E-Sail [28, 29]. In particular, the thrust model by Huo et al. [28], which is consistent with a flat E-Sail with a uniform electrical voltage, corresponds to when $\eta = 1$ and

$$\gamma = \sqrt{1 - \frac{3}{4}\,\sin^2\alpha_n} \quad , \quad \alpha = \arctan\left(\frac{\sin\alpha_n\,\cos\alpha_n}{1+\cos^2\alpha_n}\right) \tag{6}$$

where $\alpha_n \in [-90,\, 90]\,\text{deg}$ represents the angle between $\hat{\boldsymbol{i}}_r$ and the E-Sail spin axis. In this model, $\alpha_{\max} = \arctan\left(\sqrt{2}/4\right)\,\text{rad} \simeq 19.47\,\text{deg}$ and $\gamma \in [0.5,\, 1]$ cannot be written as an explicit function of α. The propulsive acceleration provided by a MagSail [30, 12, 11] may also be modeled through Eq. (5), as it will be clarified later on.

Using the expression of $\boldsymbol{a}$ given by Eq. (5), the last two of Eqs. (3) become

$$\dot{v}_r = -\frac{\mu_\odot}{r^2} + \frac{h^2}{r^3} + a_c\,\gamma\,\left(\frac{r_\oplus}{r}\right)^\eta\,\cos\alpha \tag{7}$$

$$\dot{h} = a_c\,\gamma\,r_\oplus^\eta\,r^{1-\eta}\,\sin\alpha \tag{8}$$

Even though the system of differential equations given by the first two of Eqs. (3) and Eqs. (7)-(8) has no general solution, an analytical approximation of the time-variation of the spacecraft states will now be obtained with suitable simplifying approximations.

3. Generalized sail trajectory approximation

The spacecraft propelled trajectory may be calculated by introducing two simplifying assumption. The first one is to consider a low-performance propulsion system, that is, a generalized sail such that the propulsive acceleration magnitude $\|\boldsymbol{a}\|$ is a small fraction of the local Sun's gravitational acceleration $\mu_\odot/r^2$, viz.

$$\frac{a_c\,\gamma\,r_\oplus^\eta\,r^{2-\eta}}{\mu_\odot} \leq \frac{a_c\,r_\oplus^\eta\,r^{2-\eta}}{\mu_\odot} \ll 1 \tag{9}$$

In the second place, we assume a constant thrust angle α along the whole flight, which amounts to stating that the generalized sail attitude remains constant in an orbital reference frame. Note that the latter assumption implies the dimensionless function γ to be a constant of motion.

Because the parking orbit is circular, and paralleling the procedure proposed by Battin [31], it is reasonable to expect that the spacecraft propelled trajectory will remain nearly circular, so that the specific angular momentum may be approximated as

$$h \simeq \sqrt{\mu_\odot\,r} \tag{10}$$

from which

$$\dot{h} \simeq \sqrt{\frac{\mu_\odot}{4\,r}}\,\dot{r} \tag{11}$$

In other terms, it is reasonable to expect that the spacecraft trajectory will roughly resemble a sort of tight spiral. Equating (8) and (11), we get the following first order differential equation in r

$$\dot{r} = \lambda\,r^{1-\beta} \tag{12}$$

where β and λ are two constants of motion defined as

$$\beta \triangleq \frac{2\,\eta - 1}{2} \quad , \quad \lambda \triangleq \frac{2\,\gamma\,\sin\alpha\,a_c\,r_\oplus^\eta}{\sqrt{\mu_\odot}} \tag{13}$$

An integration of Eq. (12) gives the approximate time-variation of the Sun-spacecraft distance, viz.

$$r \simeq \tilde{r} \triangleq \begin{cases} r_0\,\chi^{1/\beta} & \text{if} \quad \eta \neq 1/2 \\ \\ r_0\,\exp\left(\lambda\,t\right) & \text{if} \quad \eta = 1/2 \end{cases} \tag{14}$$

where $\chi = \chi(t)$ is a dimensionless auxiliary function (of time t) defined as

$$\chi \triangleq 1 + \frac{\beta\,\lambda\,t}{r_0^\beta} \tag{15}$$

Note that χ makes physical sense provided it is positive; see Eq. (14). In particular, the latter condition occurs $\forall t$ when $\beta\,\lambda \geq 0$, and for $t < -r_0^\beta / \left(\beta\,\lambda\right)$ when $\beta\,\lambda < 0$, that is, when $\alpha < 0 \wedge \eta > 1/2$ or $\alpha > 0 \wedge \eta < 1/2$.

Differentiating Eq. (14), the approximate time-variation of the radial component of the spacecraft velocity is given by

$$v_r \simeq \tilde{v}_r \triangleq \begin{cases} r_0^{1-\beta}\,\lambda\,\chi^{1/\beta - 1} & \text{if} \quad \eta \neq 1/2 \\ \\ r_0\,\lambda\,\exp\left(\lambda\,t\right) & \text{if} \quad \eta = 1/2 \end{cases} \tag{16}$$

while, bearing in mind Eq. (10) and recalling that $v_\theta \triangleq h/r$, the transverse component of the spacecraft velocity is $v_\theta \simeq \sqrt{\mu_\odot / r}$, which gives

$$v_\theta \simeq \tilde{v}_\theta \triangleq \begin{cases} \sqrt{\dfrac{\mu_\odot}{r_0}}\,\chi^{-1/(2\,\beta)} & \text{if} \quad \eta \neq 1/2 \\ \\ \sqrt{\dfrac{\mu_\odot}{r_0}}\,\exp\left(-\dfrac{\lambda\,t}{2}\right) & \text{if} \quad \eta = 1/2 \end{cases} \tag{17}$$

Finally, the approximate time-variation of the polar angle θ may be obtained by observing that, because $\dot{\theta} \triangleq v_\theta / r$ and $v_\theta \simeq \sqrt{\mu_\odot / r}$, the spacecraft angular velocity is related to the orbital radius as

$$\dot{\theta} \simeq \sqrt{\frac{\mu_\odot}{r^3}} \tag{18}$$

so that θ is the solution of the following integral

$$\theta \simeq \tilde{\theta} \triangleq \begin{cases} \sqrt{\dfrac{\mu_\odot}{r_0^3}} \displaystyle\int_0^t \chi^{-3/(2\,\beta)}\,\mathrm{d}t & \text{if} \quad \eta \neq 1/2 \\ \\ \sqrt{\dfrac{\mu_\odot}{r_0^3}} \displaystyle\int_0^t \chi^{-1}\,\mathrm{d}t & \text{if} \quad \eta = 1/2 \end{cases} \tag{19}$$

In particular, when $\lambda \neq 0$, the previous equation gives

$$\tilde{\theta} = \begin{cases} \sqrt{\dfrac{\mu_\odot}{r_0^3}}\, \dfrac{2\, r_0^\beta}{(3-2\,\beta)\,\lambda}\, \left[1-\chi^{1-3/(2\,\beta)}\right] & \text{if} \quad \eta \neq \{1/2;\, 2\} \\ \sqrt{\dfrac{\mu_\odot}{r_0^3}}\, \dfrac{r_0^\beta}{\beta\,\lambda}\, \ln\chi & \text{if} \quad \eta = 2 \\ \sqrt{\dfrac{\mu_\odot}{r_0^3}}\, \dfrac{2}{3\,\lambda}\, \left[1-\exp\left(-\dfrac{3\,\lambda\, t}{2}\right)\right] & \text{if} \quad \eta = 1/2 \end{cases} \tag{20}$$

When, instead, $\lambda = 0$, Eq. (15) gives $\chi = 1$. In that case, Eqs. (14), (16), (17), and (19) give $\tilde{r} = r_0$, $\tilde{v}_r = 0$, $\tilde{v}_\theta = \sqrt{\mu_\odot / r_0}$, and $\tilde{\theta} = \sqrt{\mu_\odot / r_0^3}\, t$, that is, the approximate trajectory coincides with the circular parking orbit. In fact, the case $\lambda = 0$ corresponds to either $a_c = 0$ or $\alpha = 0$; see Eq. (13). In the former case, the spacecraft is not subject to any propulsive acceleration and, therefore, it keeps moving along the circular (Keplerian) parking orbit. In the latter case, instead, the spacecraft is subjected to a purely radial thrust and the specific angular momentum is a constant of motion. Due to the assumption of low thrust, the spacecraft actual trajectory is constrained within an annular region, which describes the potential well introduced by Prussing and Coverstone [32].

4. Application to a MagSail-based mission scenario

The previously discussed mathematical model is now applied to approximate the propelled trajectory of a MagSail-based spacecraft in a heliocentric mission scenario. In this context, the thrust model detailed in Ref. [33] is used to describe the propulsive acceleration of a MagSail with a so-called "thick magnetopause mode", that is, a MagSail with a kilometer-size loop radius; see Fig. 1. In the rest of the work, such a MagSail will be referred to as "thick MagSail".

The thrust model of Ref. [33] describes the thick MagSail propulsive acceleration vector $\boldsymbol{a}$ though the following (compact) equation

$$\boldsymbol{a} = a_c \left(\frac{r_\oplus}{r}\right)^{4/3} \left(C_D\, \hat{\boldsymbol{i}}_r + C_L\, \hat{\boldsymbol{i}}_\theta\right) \tag{21}$$

where $\{C_D,\, C_L\}$ are two dimensionless functions of the MagSail angle of attack $\phi \in [-90,\, 90]$ deg, the latter being defined as the angle between the Sun-spacecraft line and the direction of the loop magnetic dipole moment $\boldsymbol{m}$; see Fig. 3.

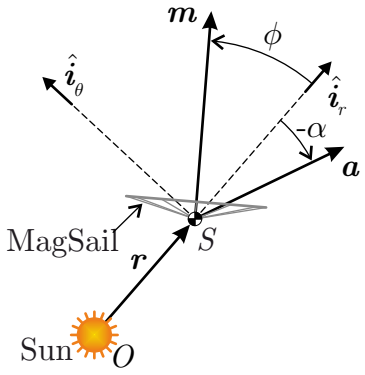

Figure 3: MagSail angle of attack ϕ.

Using a best-fit of experimental data [33], the two dimensionless functions $\{C_D,\, C_L\}$ can be written as

$$C_D = h_0 + h_1\, \cos(2\,\phi) \tag{22}$$

$$C_L = k_0\, \sin(2\,\phi) + k_1\, \sin(4\,\phi) \tag{23}$$

where $h_0 = 0.8312$, $h_1 = -0.1688$, $k_0 = -0.1338$, and $k_1 = -0.03969$ are the best-fit (dimensionless) coefficients. Note that the thick MagSail thrust model of Eqs. (21)–(23) only applies in the interplanetary space and is no longer usable when the spacecraft is located inside a planetary magnetosphere. Therefore, the (simplified) two-body dynamics described by Eqs. (3) is well suited to deal with a MagSail with a thrust model given by Eqs. (21)–(23). From Eq. (21), the expressions of $\|\boldsymbol{a}\|$ and α of a thick MagSail are

$$\|\boldsymbol{a}\| = a_c \sqrt{C_D^2 + C_L^2}\, \left(\frac{r_\oplus}{r}\right)^{4/3} \quad , \quad \alpha = \arctan\left(\frac{C_L}{C_D}\right) \tag{24}$$

so that, comparing Eq. (5) with Eq. (21) and taking into account Eq. (24), the heliocentric behaviour of a thick MagSail may be described by a generalized sail model with $\eta = 4/3$ and

$$\alpha = \arctan\left[\frac{k_0\, \sin(2\,\phi) + k_1\, \sin(4\,\phi)}{h_0 + h_1\, \cos(2\,\phi)}\right] \tag{25}$$

$$\gamma = \sqrt{\left[h_0 + h_1\, \cos(2\,\phi)\right]^2 + \left[k_0\, \sin(2\,\phi) + k_1\, \sin(4\,\phi)\right]^2} \tag{26}$$

In this context, Figs. 4-5 show the variations of $\{\alpha,\, \gamma\}$ with the angle of attack ϕ. Note that $\alpha = \alpha_{\max} \simeq 11.38\,\text{deg}$ when $\phi \simeq -29.77\,\text{deg}$, while $\gamma = \gamma_{\min} = 0.6624$ when $\phi = 0$. In addition, Fig. 6 shows the locus

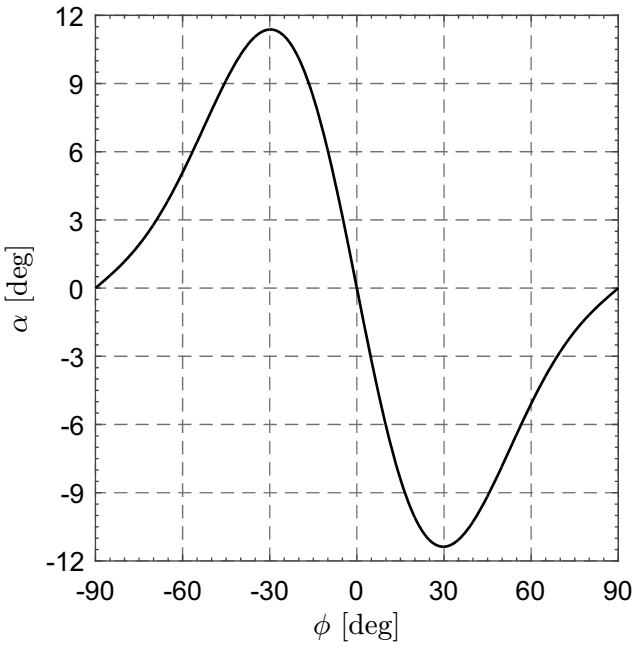

Figure 4: Variation of α with ϕ for a thick MagSail.

of all the admissible pairs $(\alpha,\, \gamma)$. Notably, a pair of values of γ exists for each value of $\alpha \neq \{-\alpha_{\max},\, \alpha_{\max}\}$, while $\gamma \simeq 0.7606$ when $\alpha = \pm\alpha_{\max}$. Moreover, both $\gamma_{\max} = 1$ and $\gamma_{\min} = 0.6624$ occur when $\alpha = 0$.

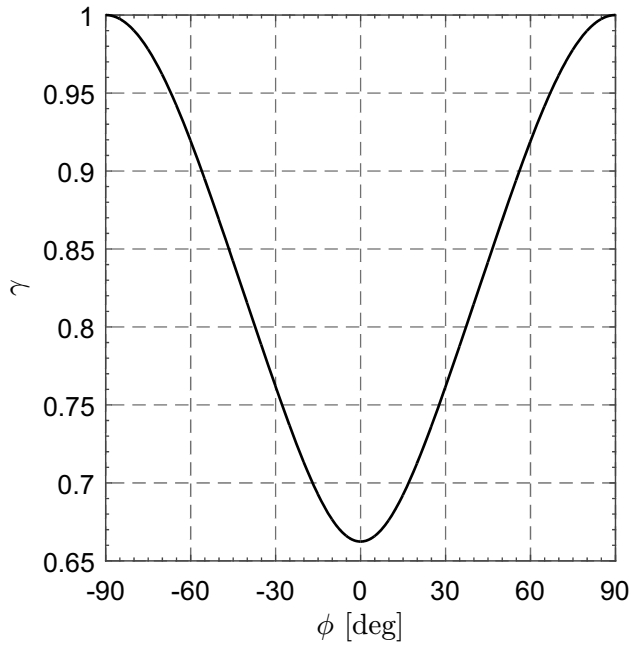

Figure 5: Variation of γ with ϕ for a thick MagSail.

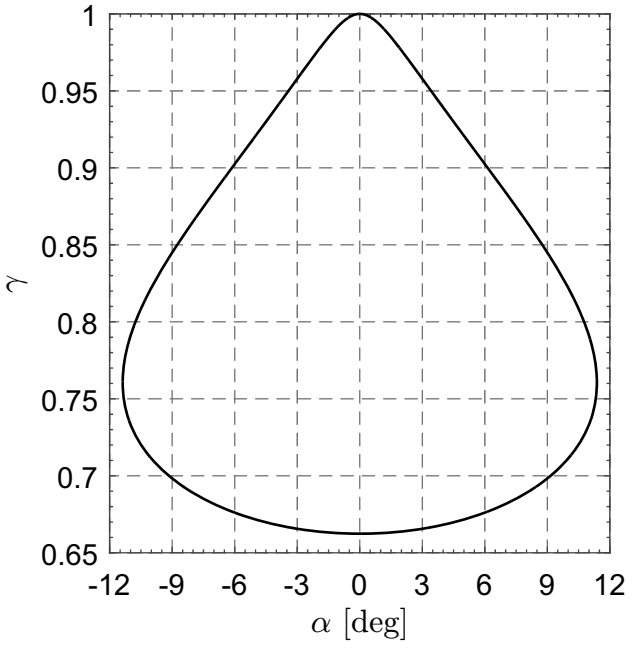

Figure 6: Locus of admissible pairs (α, γ).

In particular, when $\eta = 4/3$, Eqs. (13)–(17) and (20) give $\beta = 5/6$ and

$$\tilde{r} = r_0\,\chi^{6/5} \quad , \quad \tilde{v}_r = r_0^{1/6}\,\lambda\,\chi^{1/5} \quad , \quad \tilde{v}_\theta = \sqrt{\frac{\mu_\odot}{r_0}}\,\chi^{-3/5} \quad , \quad \tilde{\theta} = \sqrt{\frac{\mu_\odot}{r_0^3}}\,\frac{3\,r_0^{5/6}}{2\,\lambda}\,\left[1-\chi^{-4/5}\right] \tag{27}$$

where the auxiliary function $\chi = \chi(t)$ is now given by

$$\chi = 1 + \frac{5\,\lambda\,t}{6\,r_0^{5/6}} \tag{28}$$

Note that for a thick MagSail-based mission scenario the term χ is positive $\forall t$ when $\lambda \geq 0$ and for $t < t_{\max} \triangleq -6\,r_0^{5/6}/\,(5\,\lambda)$ when $\lambda < 0$.

A so small value of the maximum thrust angle (about 11 deg) corresponds to a nearly radial thrust condition. This is confirmed by Fig. 7, which shows the variation of $\gamma\,\sin\alpha$ (a sort of dimensionless component of the transverse propulsive acceleration vector, see Eq. (8)) with ϕ. In particular, the maximum (or minimum) of $\gamma\,\sin\alpha$ occurs when $\phi \simeq -33.11\,\text{deg}$ (or $\phi \simeq 33.11\,\text{deg}$) and its value is about 0.1517 (or -0.1517). The corresponding values of α are approximately equal to 11.25 deg and $-11.25\,\text{deg}$, respectively.

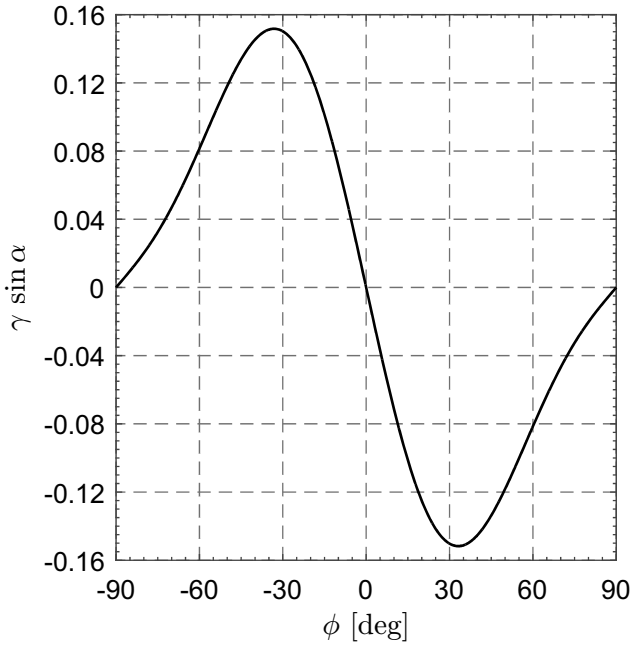

Figure 7: Variation of $\gamma\,\sin\alpha$ as a function of ϕ for a thick MagSail.

5. Model validation

The solution obtained for the thick MagSail is now validated by comparison with the results of a numerical integration of the equations of motion. The simulations are made on an 1.8 GHz Intel® Core™ i7-10510U processor using a variable order Adams-Bashforth-Moulton PECE solver [34] with absolute and relative errors equal to 10^{-12}. Such a comparison is performed by evaluating the maximum relative errors in terms of orbital radius, semimajor axis, and specific angular momentum magnitude. For an assigned value of a_c and $r_0 = r_\oplus$, the maximum relative errors are calculated as a function of $\phi \in [-90,\,90]\,\text{deg}$ during a long flight time of 100 years when $\lambda \geq 0$, or $0.99\,t_{\max}$ when $\lambda < 0$. In the latter case we have also introduced the constraint $\min\,(r) = r_{\min} \triangleq 0.25\,\text{au}$ on the minimum allowable orbital radius in order to prevent the spacecraft from an excessive thermal load due to a close passage with the Sun. Such a constraint is activated when, for an assigned value of $\lambda < 0$, there exists $\bar{t} < 0.99\,t_{\max}$ for which $r\,(\bar{t}) = r_{\min}$.

The relative errors ϵ_i, with $i = \{r,\,a,\,h\}$, are defined as

$$\epsilon_r \triangleq \frac{|r - \tilde{r}|}{r} \quad , \quad \epsilon_a \triangleq \frac{|a - \tilde{a}|}{a} \quad , \quad \epsilon_h \triangleq \frac{\left|h - \tilde{h}\right|}{h} \tag{29}$$

where a is the semimajor axis of the osculating orbit, given by

$$a = \frac{\mu_\odot \, r}{2\,\mu_\odot - r\,(v_r^2 + v_\theta^2)} \tag{30}$$

The maximum value of ϵ_i as a function of ϕ, is plotted in Fig. 8 when $a_c = \{0.05,\, 0.075,\, 0.1\}\,\mathrm{mm/s^2}$. As

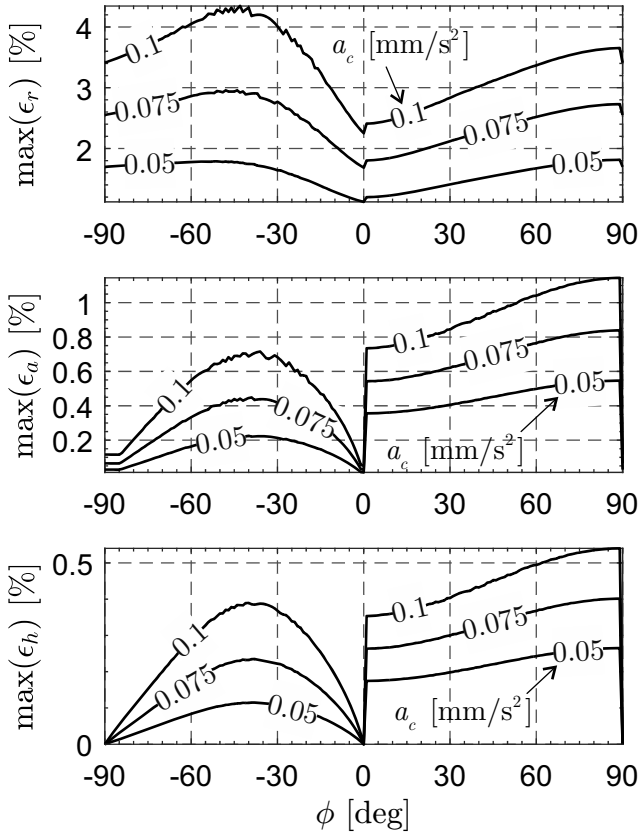

Figure 8: Maximum relative errors for $a_c = \{0.05,\, 0.075,\, 0.1\}\,\mathrm{mm/s^2}$.

expected, the maximum relative errors grow with a_c for both an orbit raising ($\phi < 0$) and an orbit lowering ($\phi > 0$). With reference to Fig. 8, the largest relative error concerns the orbital radius when $a_c = 0.1\,\mathrm{mm/s^2}$ and $\phi = -43.04\,\mathrm{deg}$. In that case, $\alpha \simeq 9.62\,\mathrm{deg}$, $\gamma \simeq 0.8313$, and $\gamma \sin\alpha \simeq 0.1389$. The comparison between the numerical (solid line) and approximate (dotted line) results when $\gamma \sin\alpha \simeq 0.1389$ is illustrated in Fig. 9(a), which clearly shows that the analytical approximations of $\{r,\, a,\, h\}$ closely follow their numerical counterparts. Finally, Fig. 9(b) shows the variation of the relative error in orbital radius during a 100-years long flight. In accordance with Figs. 8, the maximum of ϵ_r is 4.35% and occurs at $t = 100\,\mathrm{years}$.

The approximate analytical solutions ensure a considerable reduction in computational costs. More precisely, the computational savings are increasingly apparent the larger the integration time interval is. For example, when $a_c = 0.1\,\mathrm{mm/s^2}$, $\phi = -43.04\,\mathrm{deg}$, and the total flight time is 1 year, the computational cost reduces of a factor of about 30. If, instead, the total flight time is increased up to 10 years, the computational cost reduces of a factor of about 100.

6. Mission application

The previous relationships are useful for estimating the flight time t_f necessary for a thick MagSail to reach a heliocentric target orbit of semimajor axis a_f. This scenario may be used, for example, to achieve a target orbit that is synchronous with the orbit of a celestial body as a planet or an asteroid. Moreover,

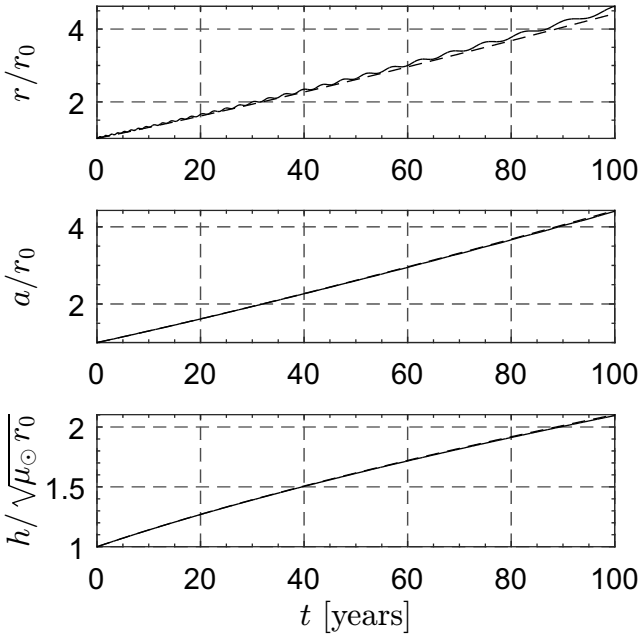

(a) Time variation of the spacecraft states.

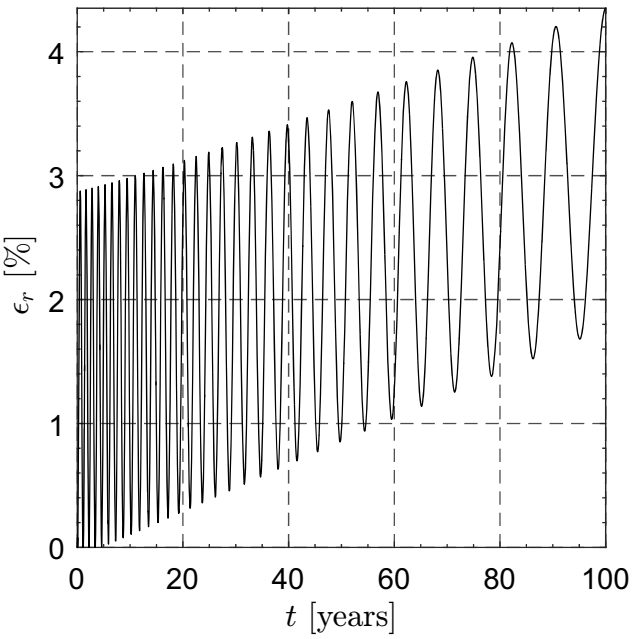

(b) Time variation of error ϵ_r.

Figure 9: Comparison between numerical (solid line) and approximate (dotted line) results.

since the eccentricity of the spacecraft osculating orbit remains small and the orbits of the planets are nearly circular, this case basically describes a circle-to-circle (two-dimensional) orbit transfer.

From Eqs. (27)-(30) it is found that the approximate flight time satisfies the equation

$$\frac{\lambda^2 r_0^{4/3}}{\mu_\odot} \chi_f^{8/5} + \frac{r_0}{a_f} \chi_f^{6/5} - 1 = 0 \tag{31}$$

with

$$\chi_f = 1 + \frac{5\,\lambda\,t_f}{6\,r_0^{5/6}} \tag{32}$$

which may be simply solved either numerically or graphically. For example, assuming $a_c = 0.1\,\mathrm{mm/s^2}$ and $\phi = -33.11\,\mathrm{deg}$ (the latter corresponding to the maximum allowable value of λ) for performing a classical Earth-Mars transfer, when $r_0 = r_\oplus$ and $a_f \simeq 1.5237\,\mathrm{au}$, the integration of the equations of motion gives $t_f \simeq 15.768\,\mathrm{years}$, whereas Eq. (31) gives $t_f \simeq 15.689\,\mathrm{years}$. In this case, the relative error in flight time is only 0.5%. The relative error in flight time is further reduced in a flyby mission towards Venus, when $r_0 = r_\oplus$ and $a_f = 0.7233\,\mathrm{au}$, assuming $a_c = 0.1\,\mathrm{mm/s^2}$ and $\phi = 33.11\,\mathrm{deg}$ (the latter corresponding to the minimum allowable value of λ). In that case, the integration of the equations of motion and Eq. (31) give $t_f \simeq 8.866\,\mathrm{years}$ and $t_f \simeq 8.830\,\mathrm{years}$, respectively, so that the corresponding relative error in flight time is only 0.4%.

In light of these results, Eq. (31) turns out to be very accurate in estimating the flight time t_f required for performing an orbital raising (or lowering) with a thick MagSail. Figure 10 shows how t_f varies with ϕ and a_f when $r_0 = r_\oplus$ and $a_c = 0.1\,\mathrm{mm/s^2}$. Note that, for a generic value of a_f, the minimum of t_f occurs when $\phi = \pm 33.11\,\mathrm{deg}$ (the sign changes according to whether it is an orbit lowering or an orbit raising), that is, when $|\gamma \sin\alpha|$ is maximum. This is confirmed by a very accurate approximation of the solution to Eq. (31), which may be obtained by neglecting the first term in the left-hand side of Eq. (31). This simplification is possible because the coefficient of the first term in the left-hand side of Eq. (31) is much less than 1 due to the assumption (9) and the observation that $|2\,\gamma \sin\alpha| < 1$ (see Fig. 7), so that

$$\frac{\lambda^2\,r_0^{4/3}}{\mu_\odot} = \left[\frac{2\,\gamma\,\sin\alpha\,a_c\,(r_\oplus/r_0)^{4/3}}{\mu_\odot/r_0^2}\right]^2 < \left[\frac{a_c\,(r_\oplus/r_0)^{4/3}}{\mu_\odot/r_0^2}\right]^2 \ll 1 \tag{33}$$

For example, when $r_0 = r_\oplus$ and $a_c = 0.1\,\mathrm{mm/s^2}$, then $\lambda^2\,r_0^{4/3}/\mu_\odot \simeq 2.6 \times 10^{-5}$. Accordingly, Eq. (31) reduces to

$$\frac{r_0}{a_f}\,\chi_f^{6/5} - 1 \simeq 0 \tag{34}$$

from which

$$t_f \simeq \frac{3\,\sqrt{\mu_\odot/r_0}}{5\,\gamma\,\sin\alpha\,a_c}\left(\frac{r_0}{r_\oplus}\right)^{4/3}\left[\left(\frac{a_f}{r_0}\right)^{5/6} - 1\right] \tag{35}$$

where $\sin\alpha < 0$ (or $\sin\alpha > 0$) when $a_f/r_0 < 0$ (or $a_f/r_0 > 0$). In particular, Eq. (35) shows that t_f is inversely proportional to $|\gamma \sin\alpha|$. This means that, for given values of r_0 and a_c, the minimum of t_f (i.e., the minimum flight time) occurs when $|\gamma \sin\alpha|$ is maximum, in accordance with the results of Figs. 7 and 10.

In this context, it is worth mentioning the recent work by Wang et al. [35], who dealt with the optimization of low-thrust Earth-orbit transfers using the vectorial orbital elements and proved the performance of the proposed dynamical model by optimizing two orbit-raising trajectories and one orbit-lowering trajectory. Note also that, according to Eq. (35), t_f is inversely proportional to a_c. Finally, Fig. 11 shows the minimum value of t_f as a function of a_f for a thick MagSail with $a_c = 0.1\,\mathrm{mm/s^2}$ when $r_0 = r_\oplus$ and $\phi = 33.11\,\mathrm{deg}$ (orbit lowering) or $\phi = -33.11\,\mathrm{deg}$ (orbit raising). In this case, the values of t_f provided by Eq. (35) nearly coincides with those obtained by numerical integration.

7. Conclusions

This paper has investigated two-dimensional heliocentric transfers performed by a generalized sail, that is, a propellantless propulsion system that provides a thrust magnitude proportional to a given power of the Sun-spacecraft distance. Under the simplifying assumptions of low characteristic acceleration, constant thrust angle, and circular parking orbit, the proposed mathematical model is able to accurately approximate the spacecraft position and velocity as a function of time. The general solution has then been specialized to the case of a kilometer-size MagSail.

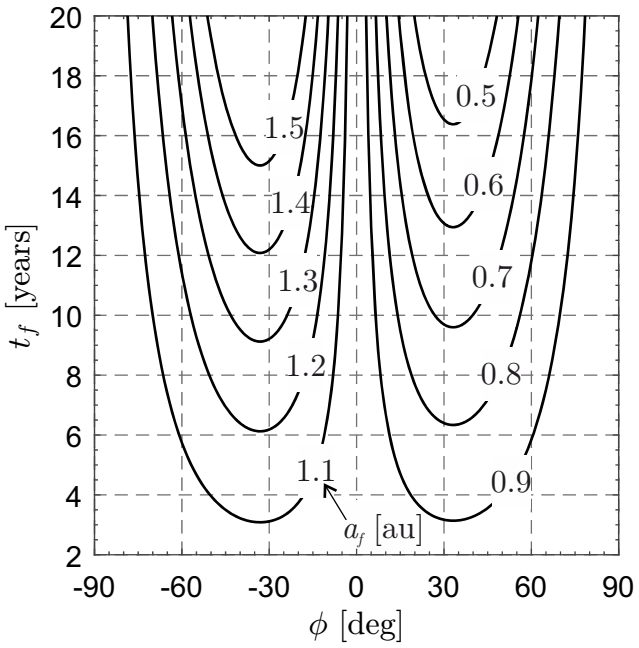

Figure 10: Flight time t_f as a function of ϕ and a_f for a thick MagSail with $a_c = 0.1\,\mathrm{mm/s^2}$ when $r_0 = r_\oplus$.

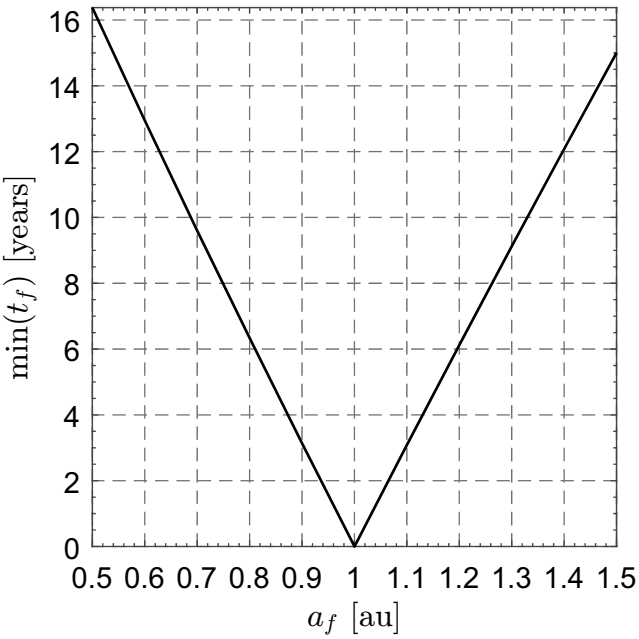

Figure 11: Minimum flight time t_f as a function of a_f for a thick MagSail with $a_c = 0.1\,\mathrm{mm/s^2}$ when $r_0 = r_\oplus$ and $\phi = 33.11\,\mathrm{deg}$ (orbit lowering) or $\phi = -33.11\,\mathrm{deg}$ (orbit raising).

The effectiveness of the proposed solution has been validated by comparison with the numerical integration of the equations of motion, which show that the analytical results approximate the actual trajectory with very small errors. The proposed mathematical model has been applied to the analysis of transfer trajectories towards a target orbit with a given semimajor axis, and an estimate of the corresponding flight time has been obtained through a closed-form expression. Based on the simulation results, it is clear that, when

dealing with the heliocentric trajectory of a generalized sail, simple analytical expressions may effectively be used to quickly estimate the evolution of the orbital parameters as a function of time. In particular, it is worth noting that the shape of the heliocentric trajectory of a generalized sail is strictly related to the exponent that describes the variation law of the thrust magnitude with the orbital radius.

8. Appendix

In this Appendix we show that the general solution of Eqs. (14)–(17) and (20) can also be applied to other (low-performance) propellantless propulsion systems. For example, the propulsive acceleration vector of an ideal photonic solar sail corresponds to when $\eta = 2$, $\alpha_{\max} = 90\,\mathrm{deg}$, and $\gamma = \cos^2\alpha$. In that case, Eqs. (14)-(20) give

$$\tilde{r} = r_0 \left(1 + \frac{3\,\cos^2\alpha\,\sin\alpha\,a_c\,r_\oplus^2\,t}{\sqrt{\mu_\odot\,r_0^3}} \right)^{2/3} \tag{36}$$

$$\tilde{\theta} = \frac{\mu_\odot/r_\oplus^2}{3\,\cos^2\alpha\,\sin\alpha\,a_c} \ln\left(1 + \frac{3\,\cos^2\alpha\,\sin\alpha\,a_c\,r_\oplus^2\,t}{\sqrt{\mu_\odot\,r_0^3}} \right) \tag{37}$$

This approximate solution is consistent with the results of Ref. [36]. Indeed, the flight time necessary to reach a target orbital radius r_f is

$$t_f \simeq \frac{\mu_\odot/r_\oplus^2}{3\,\cos^2\alpha\,\sin\alpha\,a_c} \left(\sqrt{\frac{r_f^3}{\mu_\odot}} - \sqrt{\frac{r_0^3}{\mu_\odot}} \right) \tag{38}$$

which is equivalent to Eq. (6) of Ref. [36] when the (photonic) solar sail thrust vector is described by an ideal force model without degradation [37, 38].

The second case, when $\eta = 1$, is consistent with an E-Sail thrust model [23, 39]. Using the simplified E-Sail thrust vector model of Ref. [23], where $\gamma = 1$, Eqs. (14)-(20) give

$$\tilde{r} = r_0 \left(1 + \frac{\sin\alpha\,a_c\,r_\oplus\,t}{\sqrt{\mu_\odot\,r_0}} \right)^2 \tag{39}$$

$$\tilde{\theta} = \frac{\mu_\odot/r_0}{2\,\sin\alpha\,a_c\,r_\oplus} \left[1 - \left(1 + \frac{\sin\alpha\,a_c\,r_\oplus\,t}{\sqrt{\mu_\odot\,r_0}} \right)^{-2} \right] \tag{40}$$

This solution is different from the approximate result reported by Quarta and Mengali [23]; see Eqs. (5)-(6) and (10)-(11) of Ref. [23]. The reason of this discrepancy is that the solution of Ref. [23] is obtained under the assumption $\dot{v}_r \simeq 0$, while the solution proposed in this work is found by considering $v_\theta \simeq \sqrt{\mu_\odot/r}$. Notably, Eqs. (39)-(40) provide the exact time-variation of the specific angular momentum magnitude, which is known to vary linearly over time for an E-Sail with a constant attitude [23]. In fact, observe that

$$h \triangleq r^2\,\dot{\theta} \simeq \tilde{r}^2\,\dot{\tilde{\theta}} = \sqrt{\mu_\odot\,r_0} + \sin\alpha\,a_c\,r_\oplus\,t \tag{41}$$

coincides with Eq. (5) of Ref. [23] recalling that, in our case, $\sqrt{\mu_\odot\,r_0}$ represents the specific angular momentum at the initial time.

Conflict of interest statement

The authors declared that they have no conflicts of interest to this work.

References

[1] C. R. McInnes, Solar Sailing: Technology, Dynamics and Mission Applications, Springer-Praxis Series in Space Science and Technology, Springer-Verlag, 2004.

[2] D. A. Spencer, L. Johnson, A. C. Long, Solar sailing technology challenges, Aerospace Science and Technology, Article no. 105276. 93 (2019) 1–12, doi: 10.1016/j.ast.2019.07.009.

[3] A. Farrés, J. Heiligers, N. Miguel, Road map to L_4/L_5 with a solar sail, Aerospace Science and Technology, Article no. 105458. 95 (2019) 1–16, doi: 10.1016/j.ast.2019.105458.

[4] L. Niccolai, G. Mengali, A. A. Quarta, A. Caruso, Feedback control law of solar sail with variable surface reflectivity at Sun-Earth collinear equilibrium points, Aerospace Science and Technology 106 (2020) Article number 106144, doi: 10.1016/j.ast.2020.106144.

[5] A. Caruso, A. A. Quarta, G. Mengali, M. Ceriotti, Shape-based approach for solar sail trajectory optimization, Aerospace Science and Technology 107 (2020) Article number 106363, doi: 10.1016/j.ast.2020.106363.

[6] P. Janhunen, Electric sail for spacecraft propulsion, Journal of Propulsion and Power 20 (4) (2004) 763–764, doi: 10.2514/1.8580.

[7] M. Huo, G. Mengali, A. A. Quarta, N. Qi, Electric sail trajectory design with bezier curve-based shaping approach, Aerospace Science and Technology 88 (2019) 126–135, doi: 10.1016/j.ast.2019.03.023.

[8] A. Caruso, L. Niccolai, G. Mengali, A. A. Quarta, Electric sail trajectory correction in presence of environmental uncertainties, Aerospace Science and Technology 94 (2019) 105395.1–105395.7, doi: 10.1016/j.ast.2019.105395.

[9] X. Pan, A. A. Quarta, G. Mengali, M. Xu, Linearized relative motion and proximity control of E-sail-based displaced orbits, Aerospace Science and Technology 99 (2020) Article number 105574, doi: 10.1016/j.ast.2019.105574.

[10] W. Wang, G. Mengali, A. A. Quarta, H. Baoyin, Decentralized fault-tolerant control for multiple electric sail relative motion at artificial Lagrange points, Aerospace Science and Technology 103 (2020) Article number 105904, doi: 10.1016/j.ast.2020.105904.

[11] R. M. Zubrin, D. G. Andrews, Magnetic sails and interplanetary travel, Journal of Spacecraft and Rockets 28 (2) (1991) 197–203, doi: 10.2514/3.26230.

[12] R. M. Zubrin, The use of magnetic sails to escape from low earth orbit, Journal of the British Interplanetary Society 46 (3) (1992) 3–10, doi: 10.2514/6.1991-3352.

[13] M. Bassetto, A. A. Quarta, G. Mengali, Magnetic sail-based displaced non-Keplerian orbits, Aerospace Science and Technology 92 (2019) 363–372, doi: 10.1016/j.ast.2019.06.018.

[14] G. Aliasi, G. Mengali, A. A. Quarta, Artificial equilibrium points for a generalized sail in the circular restricted three-body problem, Celestial Mechanics and Dynamical Astronomy 110 (4) (2011) 343–368, doi: 10.1007/s10569-011-9366-y.

[15] G. Aliasi, G. Mengali, A. A. Quarta, Artificial equilibrium points for a generalized sail in the elliptic restricted three-body problem, Celestial Mechanics and Dynamical Astronomy 114 (1-2) (2012) 181–200, doi: 10.1007/s10569-012-9425-z.

[16] G. Aliasi, G. Mengali, A. A. Quarta, Artificial periodic orbits around L_1-type equilibrium points for a generalized sail, Journal of Guidance, Control, and Dynamics 38 (9) (2015) 1847–1852, doi: 10.2514/1.G000904.

[17] M. Bassetto, A. A. Quarta, G. Mengali, V. Cipolla, Spiral trajectories induced by radial thrust with applications to generalized sails, Astrodynamics 5 (2) (2021) 121–137, doi: 10.1007/s42064-020-0093-6.

[18] A. D. Ogundele, Approximate analytic solution of nonlinear Riccati spacecraft formation flying dynamics in terms of orbit element differences, Aerospace Science and Technology 113 (2021) Article number 106686, doi: 10.1016/j.ast.2021.106686.

[19] K. Fujita, Particle simulation of moderately-sized magnetic sails, The Journal of Space Technology and Science 20 (2) (2004) 26–31, doi: 10.11230/jsts.20.2_26.

[20] H. Kojima, I. Funaki, Y. Shimizu, H. Yamakawa, S. Shinohara, Y. Nakayama, Experimental simulation of a plasma flow around magnetic sail, in: 29th International Electric Propulsion Conference, Princeton (NJ), October 31–November 4, 2005, paper IEPC-2005-107.

[21] Y. Kajimura, H. Usui, I. Funaki, K. Ueno, M. Nunami, I. Shinohara, M. Nakamura, H. Yamakawa, Hybrid particle-in-cell simulations of magnetic sail in laboratory experiment, Journal of Propulsion and Power 26 (1) (2010) 159–166, doi: 10.2514/1.45096.

[22] Y. Murayama, K. Ueno, Y. Oshio, H. Horisawa, I. Funaki, Preliminary results of magnetic field measurements on multi-coil magnetic sail in laboratory experiment, Vacuum 167 (2019) 509–513, doi: 10.1016/j.vacuum.2018.05.004.

[23] A. A. Quarta, G. Mengali, Trajectory approximation for low-performance electric sail with constant thrust angle, Journal of Guidance, Control, and Dynamics 36 (3) (2013) 884–887, doi: 10.2514/1.59076.

[24] L. Niccolai, A. A. Quarta, G. Mengali, Analytical solution of the optimal steering law for non-ideal solar sail, Aerospace Science and Technology 62 (2017) 11–18, doi: 10.1016/j.ast.2016.11.031.

[25] R. L. Forward, Solar photon thrustor, Journal of Spacecraft and Rockets 27 (4) (1990) 411–416, doi: 10.2514/3.26158.

[26] G. Mengali, A. A. Quarta, Earth escape by ideal sail and solar-photon thrustor spacecraft, Journal of Guidance, Control, and Dynamics 27 (6) (2004) 1105–1108, doi: 10.2514/1.10637.

[27] G. Mengali, A. A. Quarta, Compound solar sail with optical properties: Models and performance, Journal of Spacecraft and Rockets 43 (1) (2006) 239–245, doi: 10.2514/1.16003.

[28] M. Huo, G. Mengali, A. A. Quarta, Electric sail thrust model from a geometrical perspective, Journal of Guidance, Control, and Dynamics 41 (3) (2018) 734–740, doi: 10.2514/1.G003169.

[29] M. Bassetto, G. Mengali, A. A. Quarta, Stability and control of spinning E-sail in heliostationary orbit, Journal of Guidance, Control, and Dynamics 42 (2) (2018) 425–431, doi: 10.2514/1.G003788.

[30] D. G. Andrews, R. M. Zubrin, Magnetic sails and interstellar travel, Journal of the British Interplanetary Society 43 (6) (1990) 265–272 .

[31] R. H. Battin, An Introduction to the Mathematics and Methods of Astrodynamics, AIAA, New York, 1987, pp. 416–417, ISBN: 1-563-47342-9.

[32] J. E. Prussing, V. Coverstone-Carroll, Constant radial thrust acceleration redux, Journal of Guidance, Control, and Dynamics 21 (3) (1998) 516–518, doi: 10.2514/2.7609.
[33] A. A. Quarta, G. Mengali, G. Aliasi, Optimal control laws for heliocentric transfers with a magnetic sail, Acta Astronautica 89 (2013) 216–225, doi: 10.1016/j.actaastro.2013.04.018.
[34] L. F. Shampine, M. W. Reichelt, The MATLAB ODE suite, SIAM Journal on Scientific Computing 18 (1) (1997) 1–22, doi: 10.1137/S1064827594276424.
[35] Y. Wang, C. Han, X. Sun, Optimization of low-thrust Earth-orbit transfers using the vectorial orbital elements, Aerospace Science and Technology 112 (2021) Article number 106614, doi: 10.1016/j.ast.2021.106614.
[36] A. A. Quarta, G. Mengali, Semi-analytical method for the analysis of solar sail heliocentric orbit raising, Journal of Guidance, Control, and Dynamics 35 (1) (2012) 330–335, doi: 10.2514/1.55101.
[37] G. Mengali, A. A. Quarta, C. Circi, B. Dachwald, Refined solar sail force model with mission application, Journal of Guidance, Control, and Dynamics 30 (2) (2007) 512–520, doi: 10.2514/1.24779.
[38] B. Dachwald, et al., Potential solar sail degradation effects on trajectory and attitude control, in: AIAA Guidance, Navigation, and Control Conference and Exhibit, San Francisco, USA, 2005, paper AIAA 2005-6172.
[39] L. Niccolai, A. A. Quarta, G. Mengali, Two-dimensional heliocentric dynamics approximation of an electric sail with fixed attitude, Aerospace Science and Technology 71 (2017) 441–446, doi: 10.1016/j.ast.2017.09.045.